Airflow Study for a Cluster of Campus Buildings using Different Turbulence Modeling Approaches

Danko Davidovic[a,b], Jiying Liu[a,c], Mohammad Heidarinejad[d] and Jelena Srebric[a,d,*]
[a]*Department of Architectural Engineering, The Pennsylvania State University, University Park, PA, 16802, USA*
[b]*Huber Engineered Woods, Commerce, GA, 30530, USA*
[c]*School of Thermal Engineering, Shandong Jianzhu University, Jinan, 250101, China*
[d]*Department of Mechanical Engineering, University of Maryland, College Park, MD, 20742, USA*

Abstract

Obtaining accurate numerical simulations of airflows for actual building clusters is time consuming due to a vast variety of characteristic flow patterns, combined with a wide spectrum of spatial and temporal scales. In order to provide a faster, yet reliable and simple modeling approach for simulation of outdoor airflow around multiple buildings, the present study evaluated a performance of the modified zero-equation turbulence model (ZEQ). A comprehensive set of velocity field measurements in the wind tunnel experiment was conducted, and the results were used to calibrate the ZEQ model. Additional measured data are used for the validation of different turbulence modeling approaches. The performance of the modified and improved zero-equation turbulence model was compared to the revised "Kato-Launder" version of the "k-ε" model (MMK), and Large Eddy Simulations (LES) using the standard Smagorinsky Subgrid-scale model (SMG). The validation revealed a satisfactory performance of the calibrated ZEQ turbulence model in predicting streamwise mean velocity profiles, and demonstrated its comparative competitiveness with the two other turbulence modeling approaches. A less than satisfactory agreement between numerical results and measured data was identified in the prediction of vertical and lateral velocity components regardless of the turbulence modeling approach. Overall, the calibrated ZEQ turbulence model provided results that were comparable to MMK and SMG and required substantially smaller computational resources. An additional outcome of the present study is a recommendation for future research to improve performance of the calibrates ZEQ turbulence model using more advanced experimental techniques and implementation of macroscopic morphological parameters to account for realistic representation of the buildings settings in urban areas.

Keywords: Turbulent eddy viscosity, Zero-equation (ZEQ) turbulence model, Revised "Kato-Launder" turbulence model (MMK), Smagorinsky Subgrid-scale model (SMG), Airflow around multiple buildings, Wind tunnel experiment

* Corresponding author.
E-mail: jsrebric@umd.edu

1. Introduction

The airflow around buildings has been extensively studied in the last few decades both experimentally and numerically for several purposes: (a) determination of wind surface pressure distribution on building envelopes, (b) turbulent dispersion of airborne contaminants, and (c) pedestrian comfort. Three widely used numerical approaches for analyzing outdoor turbulent flow using Computational Fluid Dynamics (CFD) are based on Reynolds averaged Navier-Stokes (RANS) equation, Large Eddy Simulation (LES) and Direct Numerical Simulation (DNS) (Murakami, 1998). Unfortunately, the two-equation "k-ε" turbulence model, a typical turbulence modeling approach in RANS models, is not capable of resolving all complex features of the flow field around bluff bodies. This model typically over-predicts the size of the reattachment length behind the building and under-predicts the velocity magnitudes in wake regions (Mochida & Lun, 2008). It is well known that prediction of surface pressures is less accurate due to overproduction of turbulent kinetic energy in an impingement region (Kato & Launder, 1993). LES has been established as a standard for numerical computations of unsteady flows with complex flow structures, such as separation flows and flows around bluff bodies. However, there remain many difficulties in specifying inflow and outflow boundary conditions, grid stretching, and grid resolution for near wall treatment (Murakami, 1998; Stathopoulos, 1997; Chungloo, 2012, pp. 63-80). In other words, in order to get sufficient spatial resolution in the flow field near building surfaces, tens of millions of grid cells would be required (Letzel, Krane & Raasch, 2008; Lim, Thomas & Casto, 2009). Therefore, this numerical technique is still not entirely applicable in an engineering design because of the high computational costs, high sensitivity to the variations in initial and boundary conditions, and requirement for finer grid resolutions near the walls.

Besides RANS and LES approaches, DNS emerges as a technique capable of resolving the whole range of time and length scales in turbulent flows. However, due to limitations in computer resources nowadays, DNS is still restricted to flows with moderate Reynolds numbers, simplified geometry and relatively small calculation domains (Yakhot, Anor, Liu & Nikitin, 2006). In addition, as the most accurate modeling approaches, DNS and full scale measurements, require large involvement of human resources, instrumentation and computer support. On the other hand, less accurate and inexpensive alternatives have limitations in terms of their prediction capabilities. Therefore, the right choice and compromise between the accuracy and cost associated with modeling of wind flows around buildings is essential in meeting practical engineering needs.

The flow around a single building (bluff body) or multiple buildings has been widely studied and represents a well-established field of research in fluid mechanics (Blocken, Carmeliet & Stathopoulosc, 2007; Blocken, Stathopoulos, Saathoff & Wang, 2008; Gousseau, Blocken, Stathopoulos & Heijst, 2011; Tominaga & Stathopoulos, 2010; Santiago, Dejoan, Martilli, Martin & Pinelli, 2010; Liu, Cheng, Leung & Leung, 2011; Salim, Cheah & Chan, 2011; Petchdee & Chungloo, 2013, pp. 31-44; Tantasavasdi, Sreshthaputra, Suwanchaiskul & Pichaisak, 2009, pp. 31-46). However, most of the existing studies focused on isolated buildings or a regularly arranged array of matrix obstacles placed in relatively simple surroundings with simplified boundary and initial conditions. For example, Nozawa et al. (Nozawaa & Tamurab, 2002) predicted characteristics of wind flows around a low-rise building and computed pressure distribution on the surface of the building, which was immersed in various turbulent boundary layers. Maruyama et al. (Maruyamaa, Taniguchib, Okazakic & Taniikeb, 2008) performed a field experiment of flow around a 2.4 m. cube where the three-dimensional characteristics of the turbulent flows and the fluctuating surface pressures on the cube were examined. Shi et al. (Shi, Cuia, Wangb, Xua & Zhanga, 2008) presented a numerical simulation of wind field and contaminant dispersion in the flow over a group of buildings by LES and revealed a number of issues, such as spatial resolution and a reasonable subgrid stress model, which should be considered in applications of LES to such complex turbulent flows. In addition, a few studies investigated different CFD techniques to provide an effective and reliable approach for the evaluation of turbulent flow and the dispersion around an isolated cubic building (Tominaga & Stathopoulos, 2010; Zhang, Arya & Snyder, 1996), a tall steel building (Huang, Li & Xu, 2007), a high-rise building model with 1:1:2 shape (Yoshihide, Akashi, Shuzo & Satoshi, 2008), staggered wall-mounted cubes and staggered random arrays of obstacles with an area density of 25% (Xie & Castro, 2006), an array of wall-mounted cubes, front array of containers and a matrix of cubes (Cheng, Lien, Yee & Sinclair, 2003).

The literature review also revealed that there are limited studies available for intermediate cases, in which the buildings are close enough and the flow around the building is strongly affected by adjacent buildings (Blockena,

Stathopoulosb, Carmelietc & Hensena, 2011; Blocken & Gualtiieri, 2012; Blocken, Tominaga & Stathopoulos, 2013; Montazeri & Blocken, 2013; Janssen, Blocken & Hooff, 2013). One of the earliest numerical studies about wind flow around multiple buildings was carried out by Hanson et al. (Hanson, Smith, Summers & Wilson, 1982). This study pointed out that computer simulation is an attractive alternative to wind-tunnel testing and can provide accurate and economical predictions of large scale flow features. Remennikov et al. (2005) demonstrated the importance of accounting for adjacent structures when determining the blast loads on buildings. In addition, studying more realistic scenarios, such as a wake zone between multiple buildings in urban areas (Lateb, Masson, Stathopoulos & Bédard, 2010), requires usage of more advanced numerical tools.

Traditionally, zero-equation turbulence models (ZEQ) have been used in simulation of simplistic flows, such as shear layer flows. Cebeci-Smith and Baldwin-Lomax models are two of the most widely recognized zero-equation turbulence closures with practical significance. Zero-equation turbulence closure models also found application in modeling of indoor airflows (Chen & Xu, 1998) and have been implemented in commercially available software packages (Ludwig, 2010). These models showed acceptable performance in predictions of mean velocity flow fields for simulations of thermal comfort conditions in indoor spaces. However, this approach in turbulence modeling has not been extensively studied for simulations of outdoor airflow and contaminant dispersion mainly due to a myriad of length scales and flow patterns present in the outdoor flow around buildings. Therefore, a new model with an appropriate model constant and length scale appears as an advance in the development of numerical modeling capabilities for faster and yet more accurate predictions of outdoor flow fields using zero-equation turbulence models. Li et al. (Li, Li, Su & Zhu, 2012) provided a zero-equation turbulence model for outdoor airflow, however this model was derived for an isolated building and then applied to a regular building array. For a cluster of actual buildings, this model needs additional calibration.

The main objective of the present study is to provide a faster, yet reliable and simple modeling tool for simulations of outdoor airflow around multiple buildings. The intent is to improve the existing zero-equation turbulence models mainly developed and used for modeling of airflow in indoor environments. The wind tunnel modeling of complex airflow around four scaled student dorm buildings at The Pennsylvania State University campus has been carried out to provide the base for calibration of the coefficients in the ZEQ turbulence model. The calibrated ZEQ turbulence model has been incorporated in the CHAM's commercial CFD software package (Ludwig, 2010) and validated with additional data collected from the same wind tunnel. The performance of the calibrated ZEQ turbulence model is also compared with the revised "Kato-Launder" version of the "k-ε" model (MMK) and the standard Smagorinsky LES model (SMG) against data collected in the wind-tunnel experiment.

2. Wind Tunnel Experiment

In the present study, the wind tunnel modeling of complex airflow around four scaled student dorm buildings at the Pennsylvania State University campus has been carried out in the closed loop, low speed wind tunnel at the Department of Aerospace Engineering at The Pennsylvania State University using triple hot wire anemometry to collect the velocity time series at multiple points between the buildings. This section first describes the experiment setup and introduces the atmospheric surface layer modeling approaches used in the experiment. The information about flow field measurements is then explained in more detail.

2.1 Description for scale model of multiple buildings

Four student dormitory buildings located in the main campus at The Pennsylvania State University have been selected for experimental modeling of the airflow in the wind tunnel. Each of the four buildings is 28 m. long, 20 m. wide and 30 m. high. In order to fit the model into the available wind tunnel test section and to satisfy basic similarity criteria with the incoming flow, modeled student dorms have been scaled to 1:250 ratio. The test section of the wind tunnel is 0.6 m. wide and 0.9 m. high with a test section length of approximately 6.0 m. We estimated that adopted scaling ratio for modeled buildings blocked approximately 12% of the wind tunnel cross section area, with building heights of 21% of the wind tunnel height at testing section. Although general recommendation is to keep the blockage of wind tunnel cross section below 10%, with targeting values below 5%, adopted scaling ratio may cause some distortion effects in the flow field around modeled buildings. However, the construction and size of the triple hot wire probe used in the experiment did not allow further reduction in size of buildings because it would significantly limit the area between the buildings accessible by the anemometers. Additionally, taking into account the unrealistic of increasing the wind tunnel cross section area and limitations of reducing the size of building, in order to provide more accurate measured data, Barlow

et al. (Barlow, Rae & Pope, 1999) investigated that the measured velocities due to smaller blockage effect are over-estimated and needed to be corrected. Note that this study did not provide the corrected velocities, while further studies will focus on this procedure.

Figure 1(a) depicts the scaled student dorm building dimensions and corresponding spacing between the buildings. The buildings are mounted on the rotating table as shown in Figure 1(b) to allow the investigation of approaching wind with different incident angles. Mounted buildings with rotating tables were attached to the side wall of the test section in the wind tunnel. The focus on isothermal (neutrally stratified) flows with negligible influence of buoyancy forces caused by density differences permitted such mounting configuration. Furthermore, adopted mounting configuration also allows for the smaller scale ratio of modeled buildings while preserving dynamic similarity of the flow field.

In order to achieve dynamic similarity of the flow fields between the full-scale model and the experimental model, the Reynolds numbers should be equal. As a result, the points of flow separation and reattachment should be similar in both cases. However, this requirement cannot be satisfied easily in wind tunnels where the ratio of Reynolds numbers between the model and full scale is 10^{-3} order of magnitude, and a relaxation of similarity requirements is inevitable. Distortion of the flow and pressure distribution is considered negligible for Reynolds numbers larger than 104 for the flows over bluff bodies with sharp edges (Isyumov, 1999). Thus, it is recommended to maintain the incoming flow velocity around 10 m/s while keeping the bulk Reynolds number of the flow field around buildings large enough to preserve the flow and pressure distribution similarly:

$$\mathrm{Re} = U \cdot H / \upsilon = 10 \times 0.12 / 1.5 \times 10^{-5} \approx 80{,}000$$

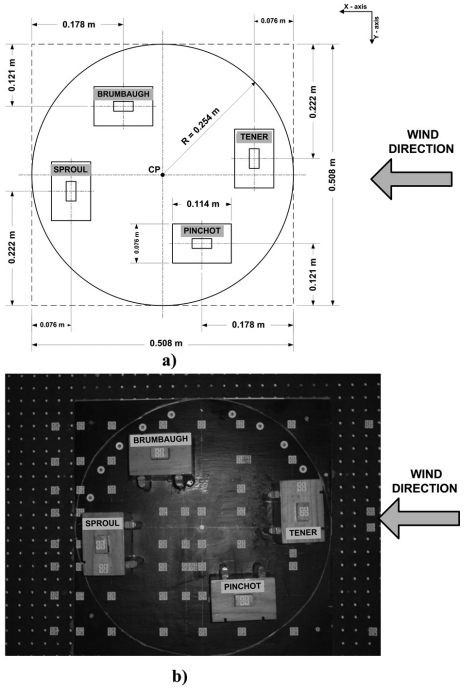

Figure 1. Four campus buildings representation with the building scaled model (plan view). (a) Model dimensions and spacing, (b) Photo of the model with marked measurement locations in the wind tunnel test section.

Moreover, the flow separation typically occurs on building corners characterized with sharp edges, and it is less affected by variation in Reynolds number. Furthermore, the reattachment points, integral turbulent length scales, and the energy spectrum of turbulence are highly dependent on the Reynolds number, and a perfect similarity with the physical model in atmospheric flow conditions cannot be easily achieved.

2.2 Simulation of ASL in the Wind Tunnel

In order to simulate the airflow around buildings properly, it is necessary to scale the properties of approaching atmospheric wind for the wind tunnel measurements by using the same scale factor that was used in modeled buildings (Cook, 1978). The simulation of the airflow around the building models in the wind tunnel was restricted only to isothermal conditions and a neutrally stable atmospheric boundary layer. Due to a relatively low height of the simulated buildings (less than 100 m.), only the lowest part of the atmospheric boundary layer, atmospheric surface layer (ASL), had to be modeled.

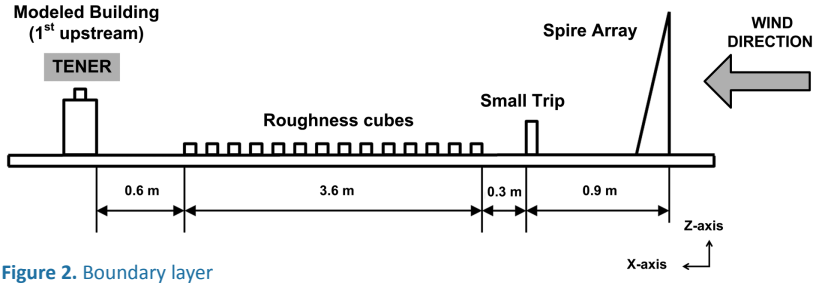

Figure 2. Boundary layer augmentation devices arrangement.

An artificial augmentation of the atmospheric surface layer in relatively short test sections of wind tunnels is typically achieved with floor roughness elements in combination with passive devices such as barriers, fences and spires (Davidovic, 2009).
In the present experiment, the floor roughness elements were represented with wooden cube elements, while the passive elements included a combination of small trip and four spires 457 mm. tall separated by 228 mm. and centered in the wind tunnel inlet. The spires were centered in the inlet of the test section 115 mm. away from the floor and ceiling of the test section. Figure 2 shows the arrangement of these boundary layer augmentation devices in the streamwise direction. The floor of the test section was covered with 19 mm. wooden cube elements in a staggered arrangement with 75 mm. of spacing between them. A total length of 3.66 m. of the test section was covered with wooden cube elements in order to increase the thickness of the boundary layer. An additional trip element made as a regular rectangular fence wall was added to this configuration to create a supplementary momentum deficit of the incoming stream and to control the boundary layer growth more precisely.

2.3 Hot Wire Anemometry Calibration and Uncertainty Estimates

The wind tunnel study utilized a three dimensional hot wire anemometry to acquire all three components of mean and turbulent velocity both in the approaching flow and in the field around scaled buildings. Hot wire anemometry is well known as a measurement technique with good spatial and time resolution, and has been established as a reliable and versatile technique for velocity measurements in flow fields with low to moderate turbulence intensities. To evaluate directional response of the hot wire probe, static velocity calibration process was carried out in round jet calibration facility with a Pitot-tube as a reference device and variable control speed fan, which allowed adjustment of the flow through jet pipe to desired magnitude. This study varied the pitch and yaw angle of the hot wire probe from -35° to + 35° in five degrees increments and collected individual wire voltage responses in each position by varying the jet speed from 0 to 25 m/s (24 velocity points in total). The data collected during the calibration process form four-dimensional cloud of points for each channel voltage of triple hot wire probe (CH1, CH2, and CH3) as a function of the velocity magnitude (V), pitch angle (α) and yaw angle (β), i.e.: ECH = f(V, α, β) indicating that the total of 15x15x24 = 5040 calibration points was generated for each channel. This study specified a denser grid of reference velocities at the low speed range, below 10 m/s, to provide a better resolution of triple hot wire sensor in the velocity ranges expected to conduct these measurements in the wind tunnel experiment.

Although relatively simple by design and underlying physics, the hot wire anemometry is subject to various sources of uncertainty, such as probe disturbance, deficiencies in conversion process from recorded voltages to velocity time histories, errors caused by signal conditioners and amplifiers, and most importantly errors originated from high turbulence intensities in the flow and incapability of a hot wire probe to resolve reverse flows (Bruun, 1995). Typically, the conversion process of recorded voltages to corresponding velocity components is achieved using either the effective velocity approach or by using a look-up method. The complexity in using

effective velocity approach amplifies with number of hot wires mounted on the probe that results in increased uncertainty levels. If applied properly, look-up method can generate more accurate data.

The look-up matrix method (or direct interpolation method) deploys direct relationship between voltage pairs $(E_1(i), E_2(j), E_3(k))$ and corresponding velocity field $(V_T(i,j,k), \alpha(i,j,k), \beta(i,j,k))$. However, the process of look-up matrix generation with a high resolution of spatial data sets also may become very time consuming. Different methods are proposed for interpolation of measured points that fall between the calibration points, such as linear, bilinear interpolation, interpolation with second order Taylor series expansion, cubic spline interpolation, and interpolation with Bézier curves. Each of these methods requires usage of sophisticated mathematical tools during conversion process, and in order to avoid difficulties associated with the conversion process, this study implemented a procedure using the Delaunay triangulation method (Delaunay, 1934) and grid interpolation procedure embedded in MATLAB for interpolation of recorded voltage time series to velocity. We estimated the uncertainty and quality of the interpolation procedure by using the same spatial data set of channel voltages acquired during the calibration process as an input to developed MATLAB code for conversion of the measured voltages to velocity. As a result of this analysis, the maximum observed difference in velocity magnitude between sets of calibration velocity data and recalculated calibration velocities was around 0.3-0.35 m/s only for two calibration points from the whole data set of 5040 points. On average, discrepancies between the calibration and recalculated velocities magnitudes remained below 0.1 m/s for the majority of calibration points indicating potential uncertainty of 10% in velocity magnitude estimates for the extremely low velocity range (1 m/s or smaller), with improved accuracy down to 1% for the higher velocity range flows (10 m/s or higher). Performed analysis for uncertainty estimates, however, did not consider directional accuracy of implemented algorithm, i.e. the accuracy of implemented algorithm during decomposition of recalculated velocity vectors into three primary components along fundamental axes. This study also did not investigate in detail the response of triple hot wire and associated uncertainties in velocity estimates if the probe was exposed to reverse flows. In addition, for the calibration of hot-wire anemometer, this study accounted for the environmental influence of temperatures and pressures that were simultaneously recorded during the calibration process. Detailed information can be found in the reference (Davidovic, 2009).

2.4 Flow Field Measurements

The current study collected velocity time histories at each measurement point in the wind tunnel study for 100 s. with sampling rate of 2,000 Hz. which was sufficient to capture at least one turnover of large eddies in the flow around the buildings, and to prevent aliasing effects in the digital signal. At the same time, selected value for sampling rate provides a solid foundation for analysis of smaller turbulent micro scales, if needed. Figure 3 shows the horizontal distribution of the measurement locations, which are also indicated with white labels in Figure 1(b). Figure 4 presents the vertical distribution of the measurement locations where up to eight different velocities have been collected in vertical direction at the elevations of 25.4 mm., 50.8 mm., 76.2 mm., 101.6 mm., 133.4 mm., 152.4 mm., 177.8 mm. and 203.2 mm. The first four vertical measurement locations included the region below the modeled building heights, and the second four vertical measurement locations included the region above the buildings extending up to two building heights. This height was selected as the maximum height in the flow field most likely disturbed by the building's presence.

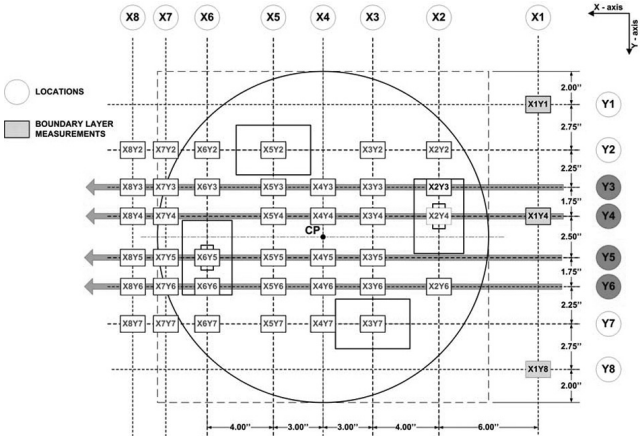

Figure 3. Distribution of measurement locations in the wind tunnel experiment (Highlighted Y3, Y4, Y5 and Y6 lines indicate data collection locations used for validation of numerical simulation results).

Figure 4. Measuring points spatial resolution in vertical direction.

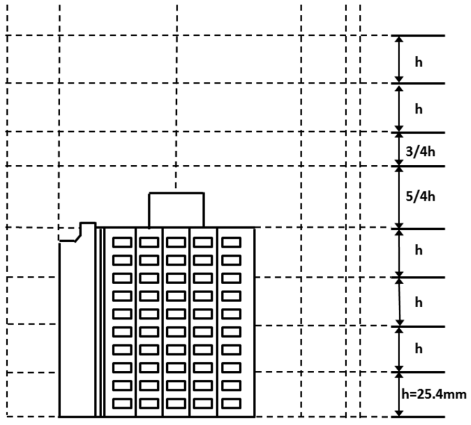

Figure 5. Inlet boundary condition-descriptions. (a)Inlet streamwise velocity profiles measured in the wind tunnel experiment, (b) Inlet turbulence intensity profiles measured in the wind tunnel experiment.

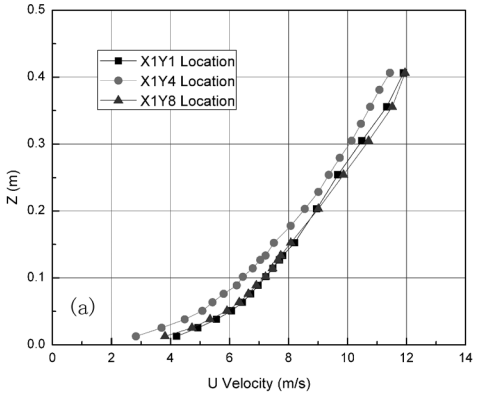

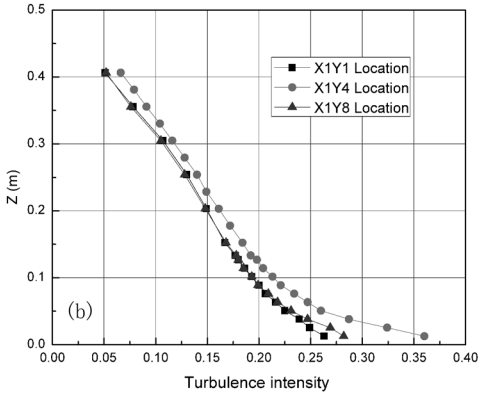

The incoming boundary conditions were measured at three separate locations 100 mm. upstream from the first building along the line X1 as defined in Figure 3. The inflow velocity and turbulence intensity were collected for 24 points in the vertical direction at the center location X1Y4, starting at 12.7 mm. above the wall and using 12.7 mm. increments in vertical direction up to the height of 127 mm. Above this point, the measurements were performed every 25.4 mm. up to the total height of 406.4 mm., which corresponds to the estimated depth of the modeled boundary layer of approximately three modeled building heights. Two corner locations X1Y1 and X1Y8 have also been investigated in more detail in order to estimate the deviation of the incoming flow velocity and turbulence intensity profile from the centerline location X1Y4 due to proximity of the ceiling and floor walls to the wind tunnel test section. Figure 5(a) demonstrates that all three measured inlet stream wise velocity profiles follow power law velocity profiles, with derived power law exponents: a_1 = 0.30 for X1Y1 location, a_2 = 0.40 for X1Y4 location, and a_3 = 0.33 for X1Y8 location. The turbulence intensity distribution along the height of the incoming wind profile is an important boundary condition for numerical simulations. Figure 5(b) shows the variation of turbulence intensity along the height at all three inlet locations observed in the wind tunnel experiment. The measured incoming wind velocity components and turbulence intensity profiles were used to specify the inlet boundary conditions in all the numerical simulations.

Calculating distribution of turbulent kinetic energy in incoming flow over various wave lengths provides a useful insight into the dominant length scales with highest energy content and interactions among different scales in the process of energy transfer. In addition, generated power spectrum curves may be used for synthetic generation of wind velocities in atmospheric surface

layers, which may be used in transient analyses deploying more advanced simulation techniques, such as LES. In order to preserve dynamic similarity, it is desirable to achieve reasonable agreement between the normalized power spectral density of incoming wind in the full scale model and modeled buildings in the wind tunnel. Unfortunately, information about the full scale properties of the modeled student dorm buildings was cost prohibitive and not readily available for comparison purposes. Thus, this study relied upon a qualitative comparison of the wind power spectra measured in the wind tunnel at three incoming locations (X1Y1, X1Y4, and X1Y8) against the power spectra reported in an existing study (Cermark, Cochran & Leflier, 1995). This previous study measured the wind power spectra both in the wind tunnel with motorized randomly oscillating vertical airfoils and in the field at Texas Tech University site (Experimental Building in Lubbock, Texas). The current study calculated the normalized longitudinal, lateral and vertical turbulent velocity power spectra at three points along the height (0.5·H, 1.0·H and 2.0·H, i.e. mid-height, roof height, and two-heights of modeled building respectively). Figures 6 to Figure 8 present the calculated power spectra for all three turbulent velocity components at building height level (1.0·H) for comparison purposes. Presented power spectrum curves have been filtered from original signal to provide smoother representation of the power spectrum curves. A closer inspection of the longitudinal power spectrum profiles shows a good correlation with identical values for the normalized frequencies where the energy peak occurs with approximately the same energy content at this frequency. In addition, the presented longitudinal power spectrum curves show very little variation between different locations except for the very low frequency end of spectrum at location X1Y8. The negative slope of the curves at higher frequencies is approximately the same and remains constant for all three inlet locations. A comparison of the lateral

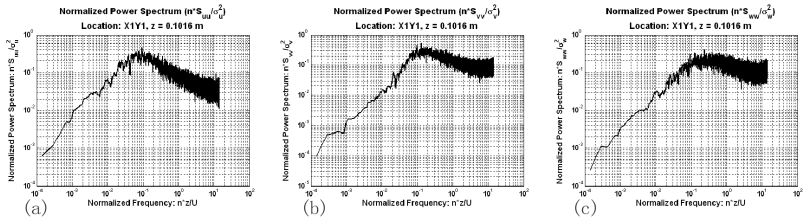

Figure 6. Normalized Longitudinal power spectrum: $n \cdot S_{uu}/\sigma_u^2$ atz = 0.1016 m.(a) Location X1Y1, (b) Location X1Y4 and (c) Location X1Y8.

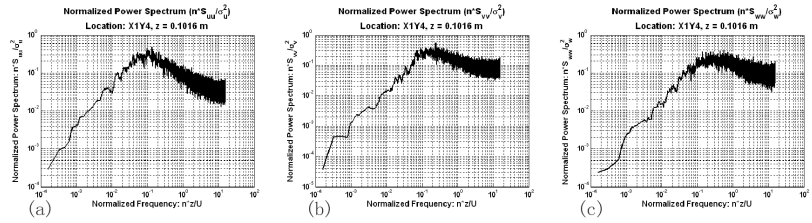

Figure 7. Normalized lateral power spectrum: $n \cdot S_{vv}/\sigma_v^2$ at z = 0.1016 m.(a) Location X1Y1, (b) Location X1Y4 and (c) Location X1Y8.

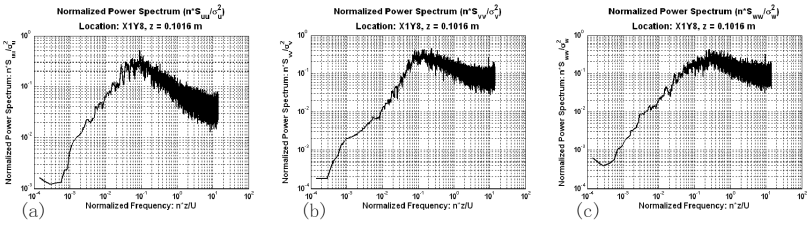

Figure 8. Normalized vertical power spectrum: $n \cdot S_{ww}/\sigma_w^2$ at z = 0.1016 m.(a) Location X1Y1, (b) Location X1Y4 and (c) Location X1Y8.

power spectrum curves indicates minor variation of the turbulent energy distribution at low frequencies for different locations and a flattening trend in the negative slope of the curve at higher frequencies. In general, curvature of the lateral power spectrum curves around the peak energy frequency is larger when compared to the curvature of the corresponding power spectrum graphs (Cermark, Cochran & Leflier, 1995). Finally, the vertical power spectrum curves show a wider energy distribution around the energy peak frequency with a minor variation at the very low frequency end for location X1Y8 when compared to the two other inlet locations. Unfortunately,

the wind tunnel and full-scale study (Cermark, Cochran & Leflier, 1995) does not provide information about the vertical power spectrum distribution. Overall, the arrangement of passive devices and roughness floor elements that the current study used in the wind tunnel test was capable of reproducing most significant characteristics of the wind in atmospheric surface layers including the longitudinal power spectrum curves. The comparison of the lateral velocity power spectrum curves reveals some discrepancies with corresponding power spectrum curves provided in the literature (Cermark, Cochran & Leflier, 1995) most likely due to the lack of more sophisticated devices for proper control of lateral turbulent velocity fluctuations, such as motor operated array of vertical airfoils installed at the inlet location.

3. CFD simulations

The numerical simulations of the flow around the four scaled student dorm buildings were carried out using the calibrated ZEQ turbulence model, the revised "Kato-Launder" version of the "k-ε" model (MMK), and the standard Smagorinsky LES model (SMG). The data obtained from the wind tunnel experiments provided a benchmark to assess the quality of numerical predictions using these three turbulence modeling approaches. This section introduces a brief description of these turbulence modeling approaches with focus on the calibrated ZEQ turbulence model.

3.1 Improved Zero-Equation Turbulence Model

Traditionally, zero-equation turbulence models have been used in simulations of simplistic flows, such as boundary layer shear flows and rely on an analogy between molecular diffusion transport and turbulent mixing. In order to maintain dimensional requirements with kinematic molecular viscosity (ν), the turbulent viscosity is proportional to a characteristic velocity and length scale:

$$\mu_t \propto C \times Velocity \times Length. \quad (1)$$

This modeling approach is based on the assumption that most of the kinetic energy from turbulence is contained in the largest eddies whose size is described with characteristic length scale. These two scales are inherent properties of the analyzed flow case studies, and are usually derived as empirical functions either from the field observations or wind tunnel experiments. The weakness of this approach is in the assumption that the turbulent viscosity is a scalar property of the local point in the flow field. This may not be valid in non-homogeneous and fairly anisotropic turbulent flows unless additional calibration coefficients (C) with more versatile properties are introduced into the turbulent viscosity equation:

$$\mu_t \propto C \times Velocity \times Length \quad (2)$$

A proper choice of the characteristic velocity, length scale, and calibration coefficients ensures a more accurate performance and better prediction of velocity and pressure fields in turbulent flows. Early attempts used the Prandtl-Kolmogorov assumption and defined the turbulent viscosity as the product of turbulence kinetic energy, k, and turbulence macroscale, L, i.e. a proper length scale for turbulence interactions:

$$\mu_t = 0.5478 \cdot \rho \cdot k^{1/2} \cdot L \quad (3)$$

where ρ is the bulk air density (kg/m3), and 0.5478 is the calibration constant. However, this approach requires either an algebraic prescription or a solution of additional conservation equation for the turbulent kinetic energy and imposes additional requirements for computational resources.

A few studies on indoor airflows simplified the expression for the turbulent viscosity using mean velocity field properties (Chen & Xu, 1998):

$$\mu_t = 0.03784 \cdot \rho \cdot V \cdot L \quad (4)$$

where V represents the total local velocity in the flow field (m/s), and L is the characteristic length scale (m), usually adopted as the distance to the nearest wall surface. The proposed formulation allows for a local adjustment of turbulent properties in the flow field and accounts for the turbulent energy dampening near the walls, since the velocities near the surface approach to zero.

Modifications of available expressions for turbulent viscosity to simulate outdoor airflow and contaminant dispersion are associated with difficulties arising from a large range of length scales involved and substantially different flow characteristics between indoors and outdoors. Simplifying the assumptions for the turbulence intensity and the turbulence length scale, a previous study (Qian, 2004; Qian & Srebric, 2011, pp. 43-51) developed and validated a new algebraic turbulence model for outdoor airflow and contaminant simulation around an isolated building. The final expression for the turbulent viscosity is developed using different sets of wind tunnel data available in the existing literature:

$$\mu_t = 0.2 \cdot \left(\frac{10^5}{\mathrm{Re}_b} \right) \cdot \rho \cdot T_{i\_\inf\ low} \cdot U \cdot L \qquad (5)$$

where Re_b is the Reynolds number at the building height, $T_{i\_\inf\ low}$ is the inflow turbulence intensity at the building height, is the local mean velocity and is the length scale defined as the smallest distance to the nearest solid surface.

Further improvements of the expression for the turbulent eddy viscosity in the zero-equation turbulence model resulted in the following formulation that was derived from wind tunnel experimental data described above (Davidovic, 2009):

$$\mu_t = C(L) \cdot \rho \cdot V \cdot L \qquad (6)$$

$$C(L) = a(\mathrm{Re}_{turb}) \cdot L \cdot \exp(-b(\mathrm{Re}_{bulk}) \cdot L) \qquad (7)$$

$$a(\mathrm{Re}_{turb}) = \mathrm{Re}_{turb}^{1/3} = \left(\frac{k_{in,H} \cdot \tau_{in,H}}{\nu} \right)^{1/3}, \quad b(\mathrm{Re}_{bulk}) = \mathrm{Re}_{bulk}^{1/3} = \left(\frac{U_{in,H} \cdot H}{\nu} \right)^{1/3} \qquad (8)$$

where V [m³/s] is the mean velocity magnitude at a local point in the flow field, L [m] is the characteristic length scale (a distance to the nearest solid surface), Re_{bulk} is the bulk Reynolds number defined for the average incoming wind speed ($U_{in,H}$) at the building average height (H), Re_{turb} is the turbulent Reynolds number defined using the turbulent kinetic energy ($K_{in,H}$) and the integral time scale ($\tau_{in,H}$) at the building average height (H), and ν represents the kinematic viscosity of air. Derived expressions originate from detailed analysis of the measured flow field around the modeled buildings in wind tunnel experiment described above, and correlate only the most dominant components of the rate-of-strain tensor in streamwise direction with the corresponding components of the turbulent Reynolds stress tensor.

In the derived expression for dimensionless constant *C*, both constants (*a* and *b*) scaled down consistently to the bulk and turbulent Reynolds number of the incoming flow at the building height level using both mean and turbulent properties of the incoming wind as input parameters. In this way, the most relevant information about the mean and turbulent properties of the incoming wind is preserved and its impact is transferred to the actual flow field.

3.2 MMK k-ε Turbulence Model

Applications of the standard k-ε turbulent model to flow fields around bluff bodies often result in simulation errors, such as the overestimation of turbulence kinetic energy in the impingement region. Although a revised k-ε model, "Kato-Launder" (LK) turbulent model (Kato & Launder, 1993), resolved the problem concerning the overestimation of by modifying the expression for production of turbulent kinetic energy (P_k), the mathematical inconsistency in the modeling of Reynolds stress $-\overline{u_i' u_j'}$ and P_k still existed. Tsuchiya et al. (Tsuchiya, Murakami, Mochida, Kondo & Ishida, 1997) proposed a new revised "Kato-Launder" version of the k-ε turbulent model (MMK model), which corrected the inconsistency of the LK model by adding a modification not to the expression for P_k , but to the expression for eddy viscosity V_t.

The governing equations of continuity and momentum conservation for steady incompressible flows are expressed as follows:

$$\frac{\partial U_i}{\partial x_i} = 0 \qquad (9)$$

$$\frac{\partial (U_i U_j)}{\partial x_j} = -\frac{1}{\rho}\frac{\partial p}{\partial x_j} + \frac{\partial}{\partial x_j}\left(\frac{\mu}{\rho}\left(\frac{\partial U_i}{\partial x_j} + \frac{\partial U_j}{\partial x_i} \right) - \overline{u_i' u_j'} \right) \qquad (10)$$

where $-\overline{u_i' u_j'}$ is the turbulent Reynolds stress tensor. The equations for the production of turbulent kinetic energy P_k and the turbulent eddy viscosity V_t are given as:

$$P_k = \nu_t S^2 \qquad (11)$$

$$\nu_t = C_\mu^* \frac{k^2}{\varepsilon}, C_\mu^* = \frac{C_\mu \Omega}{S} \quad (\Omega / S < 1) \qquad (12)$$

$$\nu_t = C_\mu^* \frac{k^2}{\varepsilon}, C_\mu^* = C_\mu \quad (\Omega / S \geq 1) \qquad (13)$$

where S and Ω represent the strain and vorticity parameters defined by the following relationships:

$$S = \sqrt{\frac{1}{2}\left(\frac{\partial U_i}{\partial x_j} + \frac{\partial U_j}{\partial x_i} \right)^2} \qquad (14)$$

$$\Omega = \sqrt{\frac{1}{2}\left(\frac{\partial U_i}{\partial x_j} - \frac{\partial U_j}{\partial x_i} \right)^2} \qquad (15)$$

3.3 Smagorinsky Subgrid-Scale Model

The standard Smagorinsky Subgrid-scale model (SMG) has been widely deployed in the LES computations, although it requires that the Smagorinsky constant (Cs) must be optimized for each flow field (Murakami, 1998). Although the standard Smagorinsky model is simple and of lower computational cost when compared to the dynamic Smagorinsky model, it has been successfully applied to certain flow problems. In the standard Smagorinsky SGS model, a simple eddy-viscosity type assumption, which is analogous to the molecular diffusion transport, is used to model the effect of unresolved subgrid-scale shear stress τ_{ij} term:

$$\tau_{ij} = \overline{u_i u_j} - \overline{u}_i \overline{u}_j \tag{16}$$

where the bar symbol denotes a spatial filtering applied to the velocity components in the Navier-Stokes equations. For instance, the velocity component u_i is represented by the sum of resolved velocity component $\overline{u}_i$ and subgrid-scale (SGS) velocity component u_i' in the x_i direction. The subgrid-scale tensor is typically modeled using the eddy viscosity hypothesis as follows:

$$\tau_{ij} - \frac{1}{3}\tau_{kk}\delta_{ij} = \nu_{sgs}\left(\frac{\partial \overline{u}_i}{\partial x_j} + \frac{\partial \overline{u}_j}{\partial x_i}\right) = -2\nu_{sgs}\overline{S}_{ij} \tag{17}$$

where ν_{sgs} is the subgrid-scale eddy viscosity and $\overline{S}_{ij}$ denotes the mean strain rate tensor of resolved velocity scales. The subgrid-scale eddy viscosity is defined as:

$$\nu_{sgs} = \left(C_S \overline{\Delta}\right)^2 \left|\overline{S}\right| \tag{18}$$

Here, $|\overline{S}|$ is the resolved strain-rate tensor given by $|\overline{S}| = \left(2\overline{S}_{ij}\overline{S}_{ij}\right)^{1/2}$, the grid size $\overline{\Delta}$ is approximated as $\left(\overline{\Delta}_1\overline{\Delta}_2\overline{\Delta}_3\right)^{1/3}$, in which $\overline{\Delta}_j$ (j=1, 2, 3) denotes the spatial grid sizes in the "j" direction. The value of the Smagorinsky constant in this study was slightly relaxed, and we adopted the value of 0.12 as recommended in the literature (Yoshihide, Akashi, Shuzo & Satoshi, 2008; Murakami, 1993).

3.4 CFD Simulation Setup

The CFD simulation setup provides a summary of the computational domain description used in the analysis along with the grid distribution, boundary condition settings and numerical scheme.

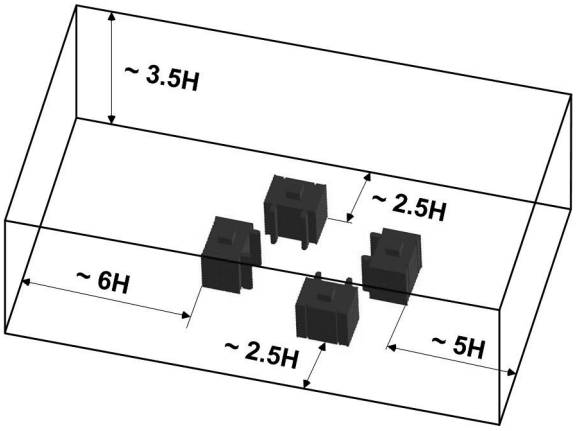

Figure 9. Locations of simulated buildings and size of numerical domain in CFD simulation.

3.4.1 Computational domain description

The simulation domain in all numerical simulations encompassed a rectangular space with constant dimensions: 1.5 m. × 0.9 m. × 0.432 m. (length × width × height). It should be noted that this domain dimensions were used according to the wind tunnel section area with blockage ration of 12%, instead of COST or AIJ guidelines (Franke, Hellsten, Schlunzen & Carissimo, 2007; Tominaga, et al., 2008). Figure 9 shows a position of the four modeled buildings within the simulated domain. The selected numerical domain allows approximately 5H of open area distance upstream, 2.5H on both sides, and 6H length behind the last building, where H is the average height of simulated buildings. The height of simulated domain is about 3.5H of the average building height to properly incorporate the measured inlet velocity and turbulence intensity profiles upstream of modeled buildings.

3.4.2 Grid distribution

A grid sensitivity test was conducted to ensure the computational accuracy of the simulations with ZEQ. The grid refinement ratio "r" for three-dimensional mesh was defined as the ratio between the number of grid elements in the fine and coarse meshes.

Roache (Roache, 1998) showed that even r=1.1 is sufficient for simple meshes. Hefny et al. (Hefny & Ooka, 2009) as well as Liu et al. (Liu, Srebric & Yu, 2013) employed r=1.2 to ensure an appropriate structured grid sensitivity analysis in the wake region. Scaperdas and Gilham (Scaperdas & Gilham, 2004)) as well as Bartzis et al. (Bartzis, Vlachogiannis & Sfetsos, 2004) recommend a maximum of 1.2 for the expansion ratio. However, it was also recommend by another study (Franke, Hellsten, Schlunzen & Carissimo, 2007)

that the expansion ratio between two consecutive cells should be below 1.3 in these regions. Therefore, to keep the truncation error small, this study finally used r=1.3 to analyze the grid sensitivity in the separation and wake region and r=1.2 for grid elements in the remainder of the simulation domain. Three different grid distributions around multiple buildings for the whole domain were arranged with 105×79×82 (coarse mesh, Δ1), 130 ×100 ×102 (medium, Δ2) and 162×124×128 (fine, Δ3) grids using structured elements. The surface-averaged skin friction coefficient (C_f) for the windward surface of the first upstream building was compared between the various grid distributions. This quantitative grid verification was performed using the grid convergence index (GCI) (Roache, 1994) based on Richardson extrapolation (Franke, Hellsten, Schlunzen & Carissimo, 2007). In this study, the GCI was described as GCI [fine]=FS|ε|/(rp-1), where FS =1.25 represents the safety factor when comparing three grids, ε is the relative error between coarse and fine grid solutions, and p=2 is the order of the discretization method based on second-order discretization of all terms in space, where p = 2 is for the systems of interest (Hefny & Ooka, 2009). The results for the ZEQ simulations showed that GCI (Kato & Launder, 1993; Mochida & Lun, 2008) = 3.05%, and GCI (Mochida & Lun, 2008; Murakami, 1998) = 8.48%. It was observed that a small value of GCI index occurred when comparing medium and fine grid results. The grid distribution of 130 ×100 ×102 shows a positive performance resulting in a grid independent flow around cubes. Therefore, all of the simulations adopted this grid distribution for each wake region occurring between two adjacent cubes.

As shown in Figure 10, a structured grid (130 ×100 ×102) was deployed to discretize the computational domain for ZEQ and MMK simulations with the y+ value approximately from 50 to 100, while for SMG simulations a refined grid (320×220×150) in the immediate vicinity of the buildings heights was employed and a very small y^+ value ($y^+ \approx 1$) is achieved for wall-adjacent cells ($\approx 5\times10^{-6}$m). In addition, the averaged cell size for SMG simulations in the wake region between two adjacent cubes, regardless of the grid number adjacent to cube surfaces was approximately 0.005 m × 0.005 m × 0.005 m. The denser grid is deployed at the center region of a numerical domain, where the simulated buildings are located. The denser grid extends almost up to two

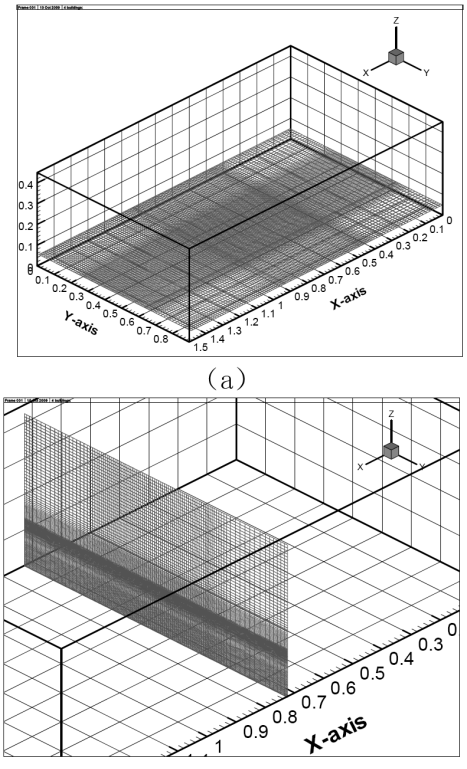

Figure 10. Thestructured grid (130 ×100 ×102) distributions for ZEQ and MMK. (a) X-Y plane, (b) Y-Z plane.

of the modeled buildings, where the largest velocity gradients and turbulence intensity are expected due to the presence of these buildings. A relatively fine grid resolution is maintained downstream of the modeled buildings to allow a proper development of the reattachment region behind the modeled buildings and to avoid potential numerical instabilities and numerically induced errors in the simulation results. The spatial discretization error for ZEQ simulations was also estimated by means

of Richardson extrapolation (Franke, Hellsten, Schlunzen & Carissimo, 2007; Roache, 1994), and is about 3% for the skin friction coefficient (C_f) of the windward surface at the first building upstream.

3.4.3 Boundary conditions

The measured inlet velocity and turbulence intensity profiles in the wind tunnel experiments were used as the inlet boundary conditions in ZEQ and MMK simulations as shown in Figure 5. A zero static pressure boundary condition was imposed at the outlet of each domain. The symmetry condition was defined at the top of the numerical domain to represent the boundary conditions at the inlet locations upstream of the modeled buildings over the entire height of the wind tunnel test section. Slip boundary conditions were utilized in lateral boundaries of the domain.

For ZEQ and MMK models, this study selected log-law wall function to resolve the viscous sub-layer, and the surfaces of the building models were modeled as roughness walls with surface roughness value around 0.0001 m. For the SMG simulation, the surfaces of the building models were modeled as perfectly smooth walls with no-slip boundaries.

For the Smagorinsky SGS model, the instantaneous fluctuation velocity components are generated by using a random number generator with the Gaussian probability density distribution obtained from the measured data:

$$f(x) = \exp\left(-(x-u)^2 / 2\sigma^2\right) / \sqrt{2\pi\sigma^2} \tag{19}$$

where σ is the inlet turbulence intensity at different heights obtained from wind tunnel experiments. All the instantaneous velocities were first calculated using Fortran program and then implemented into Q1 (input files) in the PHOENICS software (Ludwig, 2010). The time step is set to Δt = 0.0005s, which ensures that the Courant-Friedrichs-Levy(CFL) number (CFL = uΔt/Δx, where u is the local velocity magnitude and Δx is the local grid size) is always smaller than one in mostly all of the grid points, with a maximal value of 2.0 in the corner regions of buildings.

3.4.4 Numerical scheme

Three-dimensional structured mesh along with the finite volume method were utilized to discretize the computational domain and to describe the mass and momentum transport for each cell. The SIMPLEST algorithm, a variant of SIMPLE algorithm, was used to solve the system of algebraic equations for pressure and velocity components. The study also adopted the hybrid-differencing scheme for the ZEQ and MMK turbulence modeling approach to discretize momentum and pressure equations. This numerical scheme combines the first order upwind-differencing scheme in high convection regions and the second order central-differencing scheme in low convection regions. Compared with ZEQ and MMK models, SMG requires a finer spatial resolution, a smaller time increment and the central differencing scheme is recommended option for LES simulations when the cell Peclet number is lower than 2 (Ludwig, 2010). Therefore, this study applied the second order central-differencing scheme for discretization of pressure and momentum equations. The simulations achieved convergence when the mass balance was approximately within 1% of the mass flow rate for the whole domain.

4. Results

The total computation time for these three turbulence modeling approaches (ZEQ: MMK: SMG) scaled approximately to a 1:1.5:25 ratio. The velocity profiles calculated along the building height were selected to make the comparison between the numerical simulations and wind tunnel experimental data. The comparison focused on the four most representative lines in streamwise direction (Y3, Y4, Y5 and Y6) as highlighted in Figure 3. The validation process excluded several measurement locations in the wake regions behind the buildings, such as X3Y3, X3Y4, X7Y5, X8Y5, X7Y6 and X8Y6 due to the low quality of measured data at these locations, which due to the incapability of the triple hot-wire anemometer to capture complex flow features properly, especially for the reverse flows. In addition, the processing of experimental data for the vertical velocity component (W) along downstream lines Y5 and Y6 revealed anomalies indicating an unknown source of error in collected results for this velocity component along these two lines. For that reason, the following sections do not contain qualitative and quantitative comparisons between the numerical and experimental results for the vertical velocity component (W) along line Y5 and line Y6.

4.1 Results along Line Y3

Figures 11(a)-11(d) present comparisons of the mean velocity profiles for three velocity components (U, V, W) using MMK, SMG, ZEQ and experimental data along line Y3. The calculated velocity profiles for streamwise velocity component (U) show a good agreement with measured velocity profiles for all three turbulence modeling approaches, except for the X6Y3 location in the region below the mid-height of the modeled buildings. The results also show an oscillation in the streamwise velocity

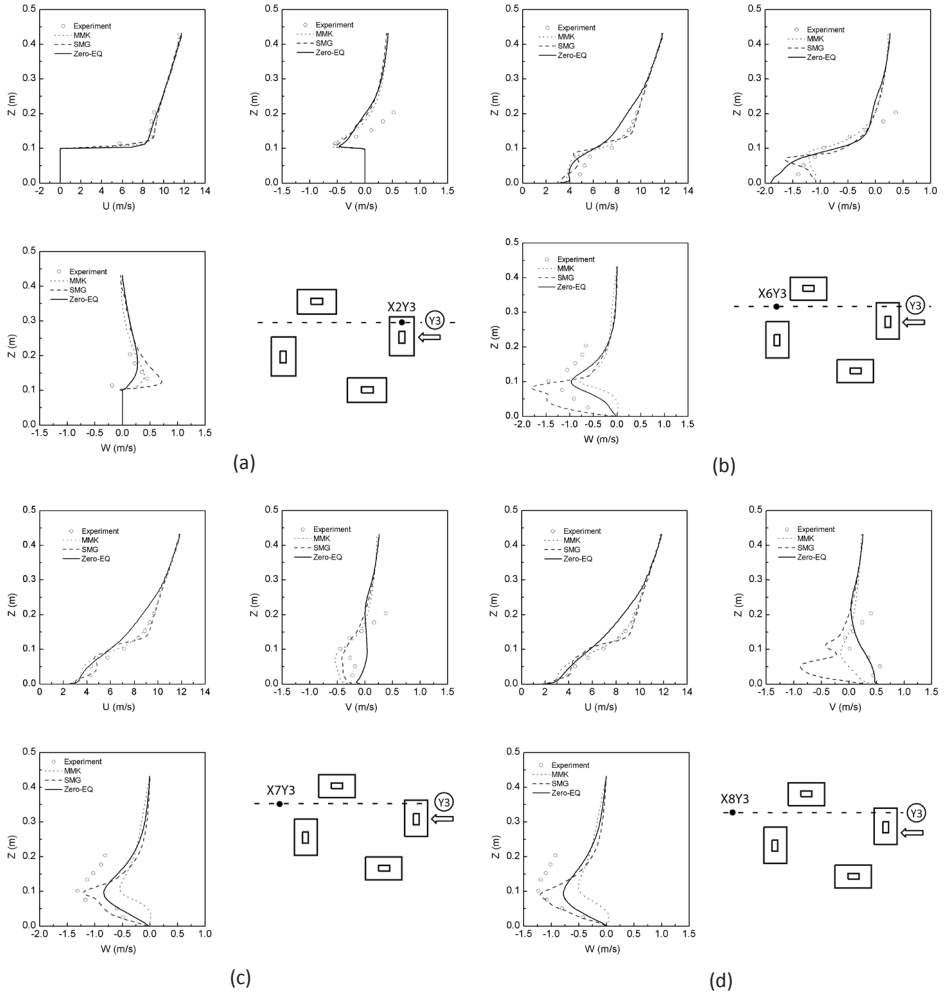

Figure 11. Downstream line Y3: Streamwise velocity component (U), Lateral velocity component (V), Vertical velocity component (W). (a) X2Y3, (b) X6Y3, (c) X7Y3, (d) X8Y3.

profile below the building height predicted by SGS for locations X7Y3 and X8Y3 compared to experimental data. MMK model shows slightly better performance than ZEQ model at the locations X7Y3 and X8Y3 as shown in Figure 11(c) and 11(d). In summary, both ZEQ and MMK turbulence models captured the general trend of the streamwise velocity profile in these regions reasonably well. Nevertheless, the ZEQ models results in a larger streamwise velocity deficit in the region above the building height than the results obtained with the MMK turbulence model, compared to experimental data."

The calculated lateral velocity component (V) profiles for the upstream locations X2Y3 above the first building exhibits the largest departures from the experimentally determined velocity profile. Interestingly, all three turbulence modeling approaches predicted similar lateral velocity profiles at this location, although the departure from the experimental data becomes more pronounced at larger heights. Overall, all approaches were capable of reproducing the curvature and profile of the lateral velocity profiles acceptably well at this location. On the one hand, ZEQ shows relatively good agreement with measured lateral velocity (V) profiles at location X6Y3, particularly at a building height level when compared with the other two approaches. On the other hand, the predicted lateral velocity profile at

location X7Y3 using MMK exhibits lower discrepancy with the experimental data, and it shows better correlation with the SMG model results. However, it appears that all turbulence modeling approaches exhibited relatively larger departures from the experimental data for the lateral velocity profile at location X8Y3. This location is placed in the wake region behind the last building and it is most likely characterized with complex velocity patterns, therefore the observed discrepancy between experimental and numerical results is not unexpected.

The strongest agreement between the wind tunnel experimental data and all simulated velocity profiles for vertical velocity component (W) exists at the upstream location X2Y3 above the top of the first building where the flow is relatively simple. All calculated velocity profiles for the vertical velocity component (W) using ZEQ follow the trend of measured velocity profiles, while slightly underpredicting the magnitude of vertical velocity peaks at downstream locations X6Y3, X7Y3 and X8Y3. Overall, the calculated vertical velocity profiles using MMK and SMG turbulence modeling approaches show a relatively poor agreement with the experimental data.

4.2 Results along Line Y4

Figures 12(a)-12(e) compare the mean velocity profiles calculated by MMK, SMG, and ZEQ turbulence models with experimental data along line Y4. Line Y4 is the centerline of the simulated domain and is of interest for investigating the quality of turbulence modeling approaches in prediction of mean velocity profiles. All three simulated profiles for the streamwise velocity component (U) at upstream location X2Y4 demonstrate a good agreement with the measured velocity profile. In particular, the ZEQ turbulence model outperformed the other two modeling approaches with a better prediction of the velocity profile shape at the building rooftop as shown in Figure 12(a). Due to compleity of the flow and turbulence fields in the wake region behind the upstream buildings, the accuracy of all three turbulence modeling approaches is reduced downstream. None of the turbulence modeling approaches reproduced the streamwise velocity profiles in the region below the building height at almost all downstream locations X4Y4, X5Y4, X7Y4 and X8Y4. The discrepancy was larger for the locations closer to the buildings (X4Y4, X7Y4 and X8Y4) while a slightly better agreement was obtained for locations characterized with fewer flow disturbances (X5Y4). Again, the SMG turbulence modeling approach resulted in more pronounced oscillatory behavior in the regions below the building height, which was not detected in the wind tunnel experiment and with other two turbulence models.

The lack of accuracy in predictions of the lateral velocity profiles (V) observed along line Y3 is also evident in the processed data for line Y4. The discrepancy was most pronounced for location X2Y4, where all turbulence modeling approaches predicted small negative velocities even though the wind tunnel experiment resulted in positive measured velocities. A slightly better agreement with the measured velocities was achieved at location X4Y4 and X5Y4 using ZEQ and MMK turbulence models, although the numerical results could not replicate the exact location of peak velocities measured in the wind tunnel experiment. Modeled velocity profiles at downstream locations in the wake behind the last building (location X7Y4 and X8Y4) demonstrated inconsistent results with different turbulence modeling approaches. The SMG turbulence model produced the closest match with the experimental data at location X7Y4, while the ZEQ turbulence model provided almost a perfect agreement with the experimental velocity profile close to the ground at location X8Y4. A departure from the experimentally determined lateral velocity profiles is exhibited in the upper regions above the building height in all three simulated velocity profiles.

The simulated mean vertical velocity (W) profiles using MMK, SMG and ZEQ at the upstream location X2Y4 demonstrate a remarkably strong agreement with the measured velocity profile. It appears that the SMG turbulence model outperformed the other two turbulence models at this location. The accuracy of numerical simulations drastically decreased for downstream locations behind the first upstream building (locations X4Y4 and X4Y5) where all simulated cases exhibited a significant discrepancy between numerical and experimental results. None of the turbulence modeling approaches were able to reproduce the negative vertical velocity values recorded in the wind tunnel experiments above the building height. The SMG simulation case provided a slightly better correlation with the experimental data closer to the ground at location X5Y4 where the negative vertical velocity values were properly predicted. In addition, the results at two furthest downstream locations (X7Y4 and X8Y4) demonstrated incapability of the turbulence modeling approaches to resolve the vertical velocity profile with a high level of accuracy. Interestingly, the ZEQ and SMG turbulence modeling approaches produced negative peak velocities at approximately the same height for both locations (X7Y4 and X8Y4), while the MMK turbulence model showed a tendency to match the positive peak velocity magnitude and height with the SMG simulation results for the lower regions at location X7Y4. Unfortunately,

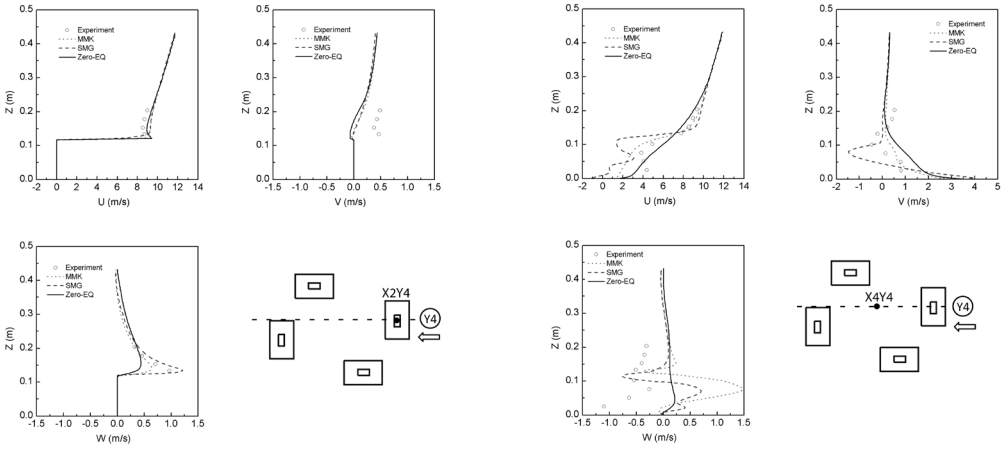

(a) (b)

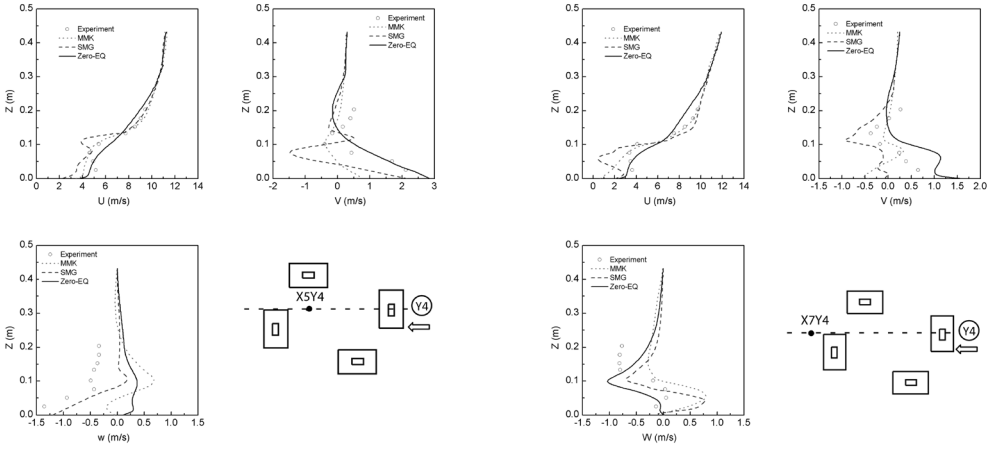

(c) (d)

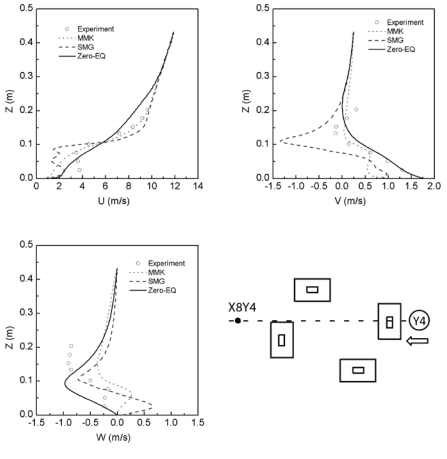

(e)

Figure 12. Downstream line Y4: Streamwise velocity component (U), Lateral velocity component (V), Vertical velocity component (W). (a) X2Y4, (b) X4Y4, (c) X5Y4, (d) X7Y4, (e) X8Y4.

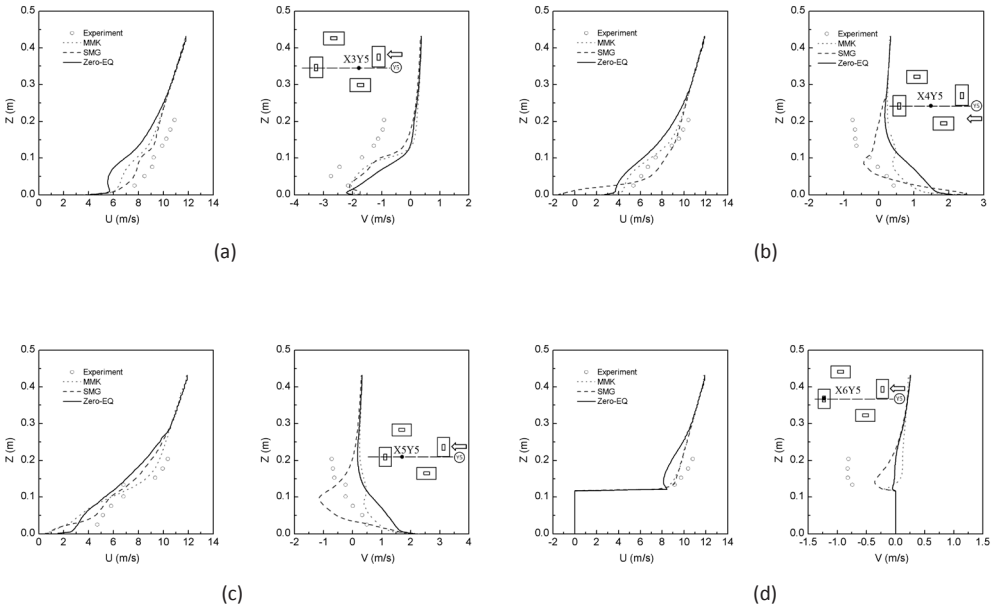

Figure 13. Downstream line Y5: Streamwise velocity component (U), Lateral velocity component (V). (a) X3Y5, (b) X4Y5, (c) X5Y5, (d) X6Y5.

none of the turbulence modeling approaches were able to replicate negative vertical velocity values in the regions above the building height as measured in the wind tunnel experiments.

4.3 Results along Line Y5

Figures 13(a)-13(d) depict the comparison between simulation results using three different turbulence modeling approaches (MMK, SMG and ZEQ) and experimental data along line Y5. Line Y5 together with line Y4 impose the most challenging modeling requirements for predicting complex flow features such as the separation, vortex shedding, tunneling effect, and reattachment of the stream. In general, the predicted streamwise velocity profiles (U) show a relatively good correlation with the observed velocity profiles in the wind tunnel experiments. Location X3Y5 is partially positioned in the separation and vortex zone behind the leading edge of the first upstream building. The numerical results for this location showed a good prediction of the slope for calculated velocity profiles, except for noticeably lower velocity magnitudes when compared to measured data. The velocity deficiency is most pronounced for the simulated velocity profiles using the ZEQ turbulence model at this location. This discrepancy becomes less pronounced for the other two downstream locations (X4Y5 and X5Y5) which are positioned in the center region between the buildings. However, the near ground streamwise velocity profile predicted by the SMG turbulence model for location X4Y5 shows negative values indicating the existence of recirculation vortex that was not observed in the experiments. In this location, the ZEQ and MMK turbulence modeling approaches outperformed the SMG large-eddy simulation approach. The simulation results for the rooftop location of the last building (location X6Y5) reveal that modeled streamwise velocity profiles did not capture completely the acceleration of the flow across this building. The velocity deficiency is most observable for the velocity profile obtained using the ZEQ turbulence modeling approach.

The simulated lateral velocity (V) profiles using all three turbulence modeling approaches demonstrated a strong agreement with measured values by successfully replicating the velocity profile development for upstream location X3Y5, although the velocity magnitudes were slightly underpredicted. In addition,

the ZEQ turbulence model successfully captured the shape and curvature of the velocity profile at locations X4Y5 and X5Y5 in the regions below the height of the modeled buildings, although the velocity magnitudes were slightly high. Nevertheless, the modeled velocity profiles using the SMG turbulence model exhibited the worst performance by showing a velocity peak close to the building height at these two locations that was not observed in the experiments. A comparison of the velocity profiles above the building height using all three turbulence modeling approaches revealed a consistent overprediction of the lateral velocity magnitude at these two locations. The predicted mean lateral velocity profile above the rooftop of the building located furthest downstream (location X6Y5) using ZEQ demonstrated a good correlation with the measured data, whereas the MMK and SMG turbulence modeling approaches revealed larger discrepancies between the simulated and measured data. Overall, the magnitude of predicted later velocities was significantly smaller when compared to the experimentally obtained velocity profiles at this location.

4.4 Results along Line Y6

Figures 14(a)-14(d) illustrate the performance of all three turbulence modeling approaches in predicting the velocity profiles along line Y6. Line Y6 represents the last in a series of lines considered in the performance evaluation process of the calibrated ZEQ turbulence model for exterior airflows. Similarly to the other three lines, line Y6 runs through the central core region between the modeled buildings and is a good representative of various flow features with a complex terrain topology.

The predicted mean streamwise velocity profile (U) at the upstream location X2Y6 strongly agreed with the measured velocity profile, although the magnitudes were consistently lower when compared to the measured data. All turbulence modeling approaches produced similar streamwise velocity profiles at this location. The SMG

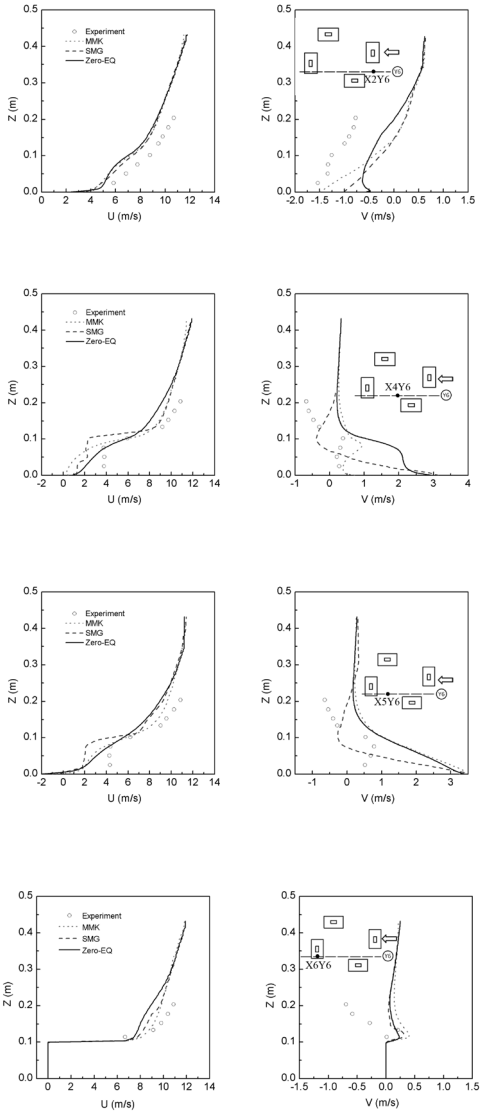

Figure 14. Downstream line Y6: Streamwise velocity component (U), Lateral velocity component (V). (a) X2Y6, (b) X4Y6, (c) X5Y6, (d) X6Y6.

turbulence model was able to accurately replicate the trend of measured velocities near the ground at locations X4Y6 and X5Y6. However, the calculated velocity magnitudes were lower when compared to the measured data. The MMK and ZEQ turbulence model produced relatively similar velocity profiles, which both showed a velocity deficiency below the building height level in comparison with the experimentally determined profiles at these two locations. All turbulence modeling approaches demonstrated the inability to accurately reproduce the measured magnitude of streamwise velocities above

the rooftop surface at location X6Y6. A similar deficiency in the streamwise velocity profile magnitude above the building rooftop was observed for the downstream location X6Y5.

A discrepancy between numerical and experimental results for the mean lateral velocities (V) was similar to the observations made for the other three lines. In general, the measured lateral velocity profiles are characterized with relatively small magnitudes that are prone to larger measurement uncertainties influencing the performance assessment of numerical simulation results. A comparison of the simulated lateral velocity profiles at location X2Y6 demonstrates a relatively similar performance of the MMK and SMG turbulence modeling approaches. On the other hand, ZEQ produced a distinctive velocity profile that better resembles the shape of the experimental velocity profile at mid-heights. However, none of the turbulence modeling approaches were capable of replicating the experimental data. The plotted velocity profiles show underperformance in predicting the magnitude of the lateral velocity component along the height.

The discrepancy between the numerically and experimentally determined lateral velocity profiles persisted at two downstream locations X4Y6 and X5Y6. The ZEQ and MMK turbulence modeling results resembled the shape of the experimental profile at location X4Y6, with a slightly better prediction of the MMK turbulence model in terms of the velocity magnitudes in the lower regions below the building height. Nevertheless, the SMG simulation results showed the largest departure from the wind tunnel experimental data at this location. All of the utilized turbulence modeling approaches failed to replicate the velocity profile and corresponding velocity magnitudes with an acceptable level of accuracy at the downstream location X5Y6. The ZEQ and MMK turbulence model produced almost identical velocity profiles with a single peak velocity value, while the SMG modeling approach generated quite a difference in shape of the velocity profile with a peak velocity occurring approximately at the building height in this location. It appears that the calculated velocity profile using the SMG turbulence modeling approach appeared to be a mirror image of the lateral velocity profile obtained in the wind tunnel experiment for this location.

None of the turbulence modeling approaches fully reproduced the velocity profile above the rooftop of the furthest building downstream at location X6Y6. In the regions above the rooftop surface, all turbulence models generated the proper shape of the velocity profile with a reasonably good agreement with the experimental data. It appears that the SMG turbulence modeling approach outperformed the other two turbulence models in this region. However, a negative lateral velocity trend along the height was not captured adequately by any of the three deployed turbulence modeling approaches.

5. Discussions

The present study compared the performance of the calibrated Zero-Equation (ZEQ) turbulence model against modified Kato-Launder "k-ε" model (MMK) and the standard Smagorinsky model (SMG). The wind tunnel simulation of the airflow around scaled student dorm buildings at the Pennsylvania State University served both as a validation study for the ZEQ turbulence model performance, and as a benchmark study to compare the performance of the three turbulence modeling approaches. The performance comparison revealed a relative competitiveness of the calibrated ZEQ turbulence model against more comprehensive turbulence modeling approaches, indicating that the ZEQ turbulence model can be selected as a faster modeling approach while remaining reliable and simple for the simulation of outdoor airflows around building clusters with complex topologies.

At several measurement locations, the ZEQ turbulence model either outperformed or at least demonstrated equivalent performance as the other two more comprehensive turbulence modeling approaches, such as the streamwise velocity shown in the Figure 12(a). Such performance of the ZEQ turbulence model indicates a promising potential to utilize this turbulence model as an effective tool in engineering practice of outdoor airflow studies. Properly calibrated coefficients in the equation for turbulent viscosity in the ZEQ turbulence model may generate a solid foundation for reliable estimates of the mean velocity fields in outdoor airflows through complex urban settings. There were a few instances where the MMK turbulence modeling approach demonstrated a better agreement with the wind tunnel experimental data. However, this study could not identify a consistent pattern with regards to specific flow features at particular measurement locations for which the MMK turbulence model outperformed the ZEQ turbulence model. The numerical results obtained using the SMG turbulence modeling approach demonstrated more pronounced oscillations of the mean velocity profiles particularly in the wake regions. However, this modeling approach is also proved to be reliable tool with acceptable levels of accuracy in predicting the

mean velocity profiles at most observed locations in this study. The source of uncertainty in the modeled results using SMG turbulence model most likely originates from insufficient resolution of input data, lack of information at the domain inlet, as well as in the necessity for further calibration of the coefficients in the expression for the subgrid scale turbulent shear stresses using eddy-viscosity hypothesis. In addition, the accuracy of simulated velocity fields depends on the velocity fluctuation at the inlet boundary (Hu, Ohba & Yoshie, 2008; Ramponi & Blocken, 2012a; Ramponi & Blocken, 2012b). It is possible that the accuracy issues for the w-velocity that all models have exhibited have come from the inlet boundary conditions for this velocity component. This critical boundary condition deserves significant investment in time and effort in future studies.

Overall, all three turbulence modeling approaches achieved the best agreement with experimental results in prediction of the streamwise mean velocity profiles. An effort invested in detailed assessment of the calibration coefficients in the algebraic relation for the turbulent eddy viscosity resulted in satisfactory performance of the ZEQ turbulence model in prediction of the streamwise velocity profiles in the current study. However, the methodology for calibration of the coefficients in the expression for turbulent eddy viscosity in the ZEQ model considered only the streamwise mean velocity gradients in the vertical direction and corresponding covariant component of the turbulent Reynolds stress tensor, neglecting the gradient of vertical velocity component in the streamwise direction due to extremely coarse spatial resolution of the measurement locations in that direction. In addition, the calibration process did not consider in detail the anisotropic properties of turbulence by analyzing the other components of the turbulent Reynolds stress tensor and corresponding components of the mean strain rate tensor. A narrow focus in the calibration process most likely affected the capabilities of the ZEQ turbulence model to predict velocity profiles for the other two mean velocity components with a greater degree of accuracy.

This study found a less acceptable agreement between the numerical results and the wind tunnel experimental data for the vertical mean velocity component profiles. Such performance of the ZEQ turbulence model is not unexpected due to partial focus on specific components of the mean strain rate tensor and corresponding turbulent Reynolds stresses during the derivation process of calibration coefficients. In general, all turbulence modeling approaches demonstrated the worst prediction capabilities for the lateral velocity component profiles. At this point, we could not identify with a great confidence the underlying cause for this discrepancy. In general, the magnitudes of mean lateral velocities are very small compared to other two velocity components, and it may be possible that even small perturbations in the approaching flow may significantly affect the flow in the lateral direction causing large uncertainty in simulations of the flow around modeled buildings. The design of triple hot-wire probe certainly imposed some limitations in ability of the sensor to resolve properly all complex flow features in the wake regions behind modeled buildings, creating an additional source of uncertainty for processed data from the wind tunnel study. Using more advanced experimental techniques may provide a more reliable tool for collection of the velocity data that will better resolve complex flow features in these critical regions. Collection of higher quality experimental data with more advanced measurement techniques, such as PIV, should form a sound basis for further refinement of the calibration coefficients in the ZEQ turbulence model. These improvements should include mean strain rate components and corresponding components of the turbulent Reynolds stress tensor that we neglected in this study.

Based on the discussed issues, the present numerical and experimental study identifies the following two critical areas for future research:

(a) Perform additional comprehensive experimental studies to collect reliable data for all components of the mean strain rate tensor and corresponding components of the turbulent Reynolds stress tensor
(b) Redefine the expressions for the calibration coefficient in the equation for the turbulent eddy viscosity to incorporate morphologic parameters of urban settings.

A detailed resolution of the flow field would require usage of more advanced experimental techniques, such as the pulsed-wire anemometry (PWA) and/or noninvasive experimental techniques including Laser Doppler Anemometry (LDA) and Particle Image Velocimetry (PIV). These measurement techniques offer more comprehensive insight into the flow features around building clusters and can supply reliable data on the energy content of turbulent eddies.

Development of more comprehensive formulations for the calibration coefficients in the expression for turbulent eddy viscosity may include an assessment of the urban area's morphologic properties and their impact on the proposed formulation for calibration coefficients. Dependency on typical scaling parameters commonly used to describe the macroscopic features of the boundary layer flows over surface roughness obstacles immersed in the atmospheric surface layer (ASL) such as the roughness length (z_0), displacement length (d) and friction velocity (u*) are preferable choices among the other variables used to characterize the atmospheric boundary layer flows, due to their unique characteristics for each particular arrangement of buildings in urban settings.

In the present equation, the turbulent viscosity expression predicted airflow around buildings in the wind tunnel using characteristic length scale expressed with distance to the nearest wall surface. While, in the real urban area, characteristic length probably results in unreasonable turbulent viscosity value. Therefore, non-dimensional characteristic length (L/H) in the new derived expression can be used to scale down inconsistency between wind tunnel buildings and real urban areas. Further study will conduct larger-scale models and larger wind tunnels to generate more accurate equations.

6. Conclusions

The examined improvements for calibration coefficient in the expression for the turbulent eddy viscosity embedded in the ZEQ turbulence model demonstrated an acceptable level of accuracy. Specifically, the velocity data calculated with the calibrated ZEQ have a relatively good agreement with experimental data obtained in the wind tunnel study of flow around four scaled student dorm buildings at The Pennsylvania State University campus. The best agreement was achieved for the streamwise mean velocity profiles along the building height throughout the flow field regardless of the turbulence modeling approach. The calibrated ZEQ turbulence model along with the other two turbulence modeling approaches, MMK and SMG, however, showed a less reliable performance in the wake regions characterized by separation, recirculation, and extreme velocity gradients.

Deficiencies identified for the ZEQ turbulence model performance may have been partially caused by the experimental instrumentation capabilities to accurately resolve the flow properties in the wind tunnel experiment. Nevertheless, the quality of predicted longitudinal (streamwise) velocity profiles by the ZEQ turbulence model was acceptable for engineering modeling purposes and of comparable accuracy to the other two more comprehensive turbulence modeling approaches used in the present study. The comparative study showed less satisfactory agreement between the numerical and experimental data for the vertical velocity component profiles, and the least accurate predictions of the calibrated ZEQ turbulence model were obtained for the predictions of lateral velocity profiles. Deficiencies observed in numerical predictions of the velocity profiles in lateral and vertical directions regardless of the turbulence modeling approach deployed are manifold. Firstly, the methodology for calibration of the coefficient in the expression for turbulent eddy viscosity in ZEQ turbulence model did not incorporate the mean strain rate tensor components for the lateral and vertical velocity components. Secondly, the experimental instrumentation used in the wind tunnel study may have not been sufficiently accurate to completely resolve the complex flow features in close proximity of the modeled buildings, particularly in the wakes and regions characterized with flow separation. Lastly, a relatively coarse grid of the measurement locations in the streamwise and lateral directions did not provide fine spatial resolution for a more comprehensive analysis and improvements in the formulation of calibration coefficients by considering other components of the mean strain rate tensor and corresponding turbulent Reynolds stresses.

Overall, when compared to other more sophisticated and more computationally demanding turbulence modeling approaches, such as modified two-equation "k-ϵ" MMK turbulence model and large eddy simulation using the Smagorinsky subgrid scale model (SMG), the current version of the ZEQ turbulence model demonstrates a competitive performance, while still providing a room for further modifications to improve its performance in modeling of the exterior airflows in urban settings.

Acknowledgements

This work was supported by the National Science Foundation (NSF) project in the Office of Emerging Frontiers in Research and Innovation (Award number: EFRI-1038264). The authors would like to express their special appreciation to Richard R. Auhl, the Research Associate in the Department of Aerospace Engineering, and Dennis K. McLaughlin, the professor in the Department of Aerospace Engineering at the Pennsylvania State University for the access to wind tunnel facility and constructive

References

Barlow, J. B., Rae, W. H. & Pope, A. (1999). *Low-Speed Wind Tunnel Testing.* New York, UK: Wiley.

Bartzis, J. G., Vlachogiannis, D. & Sfetsos, A. (2004). Thematic area 5: Best practice advice for environmental flows. *The QNET-CFD Network Newsletter, 2*(4), 34-39.

Blocken, B., Carmeliet, J. & Stathopoulosc, T. (2007). CFD evaluation of wind speed conditions in passages between parallel buildings—effect of wall-function roughness modifications for the atmospheric boundary layer flow. *Journal of Wind Engineering and Industrial Aerodynamics, 95*(9-11), 941-962.

Blocken, B. & Gualtiieri, C. (2012). Ten iterative steps for model development and evaluation applied to Computational Fluid Dynamics for Environmental Fluid Mechanics. *Environmental Modelling & Software, 33*, 1-22.

Blockena, B., Stathopoulosb, T., Carmelietc, J. & Hensena, J. L. M. (2011). Application of computational fluid dynamics in building performance simulation for the outdoor environment: An overview. *Journal of Building Performance Simulation, 4*(2), 157-184.

Blocken, B. J. E., Stathopoulos, T., Saathoff, P. & Wang, X. (2008). Numerical evaluation of pollutant dispersion in the built environment: comparisons between models and experiments. *Journal of Wind Engineering and Industrial Aerodynamics, 96*(10-11), 1817-1831.

Blocken, B., Tominaga, Y. & Stathopoulos, T. (2013). CFD simulation of micro-scale pollutant dispersion in the built environment. *Building and Environment, 64*, 225-230.

Bruun , H. H. (1995). Hot-Wire anemometry: Principles and signal analysis. USA: Oxford University Press

Cermark, J. E., Cochran, L. S. & Leflier, R. D. (1995). Wind-tunnel modelling of the atmospheric surface layer. *Journal of Wind Engineering and Industrial Aerodynamics, 54-55*, 505-513.

Cheng, Y., Lien, F. S., Yee, E. & Sinclair, R. (2003). A comparison of large Eddy simulations with a standard k–e Reynolds-averaged Navier–Stokes model for the prediction of a fully developed turbulent flow over a matrix of cubes. *Journal of Wind Engineering and Industrial Aerodynamics, 91*, 1301-1328.

Chen, Q. & Xu, W. (1998). A zero-equation turbulence model for indoor airflow simulation. *Energy and Building, 28*(2), 137-144.

Chungloo, S. (2012). Numerical Simulation of Forced Convective Heat Transfer Coefficients on Shaded Roofs with Wind Circulation in Low-Rise Buildings. *Journal of Architectural/Planning Research and Studies, 9*(2), 63-80.

Cook, N. J. (1978). Determination of the model scale factor in wind-tunnel simulations of the adiabatic atmospheric boundary layer. *Journal of Wind Engineering and Industrial Aerodynamics, 2*(4), 311-321.

Davidovic, D. (2009). *Improvements in numerical airflow modeling around multiple buildings [PhD].* PA: The Pennsylvania State University

Delaunay, B. (1934). Sur la sphère vide. A la mémoire de Georges Voronoï. Bulletin de l'Académie des Sciences de l'URSS. *Classe des sciences mathématiques et na, 6*, 793–800.

Franke, J., Hellsten, A., Schlunzen, H. K. & Carissimo, B. (2007). The COST 732 Best Practice Guideline for CFD simulation of flows in the urban environment: a summary. International *Journal of Environment and Pollution, 44*, 419-427.

Gousseau, P., Blocken, B.J.E., Stathopoulos, T. & Heijst, G.J.F. van (2011). CFD simulation of near-field pollutant dispersion on a high-resolution grid : a case study by LES and RANS for a building group in downtown Montreal. *Atmospheric Environment, 45*(2), 428-438.

Hanson, T., Smith, F., Summers, D. & Wilson, C. B. (1982). Computer simulation of wind flow around buildings. *Computer-aided Design, 14*(1), 27-31.

Hefny, M. M. & Oooka, R. (2009). CFD analysis of pollutant dispersion around buildings: Effect of cell geometry. *Building and Environment, 44*(8), 1699-1706.

Huang, S., Li, Q. S. & Xu, S. (2007). Numerical evaluation of wind effects on a tall steel building by CFD. *Journal of Constructional Steel Research, 63*(5), 612-627.

Hu, CH., Ohba, M. & Yoshie, R. (2008). CFD modelling of unsteady cross ventilation flows using LES. *Journal of Wind Engineering and Industrial Aerodynamics, 96* (10-11), 1692-1706.

Isyumov, N. (1999). *Wind tunnel studies of buildings and structures* [ASCE Manuals and Reports on Engineering Practice], 14-15. Reston, VA: Aerospace Division of ASCE.

Janssen, W. D., Blocken, B. & Hooff, T. V. (2013). Pedestrian wind comfort around buildings: Comparison of wind comfort criteria based on whole-flow field data for a complex case study. *Building and Environment, 59*, 547-562.

Kato, M. & Launder, B. E. (1993). The modelling of turbulent flow around stationary and vibrating square cylinders. *Proceeding of 9th Symposium on Turbulent Shear Flows, Kyoto, August 1993* (pp. 10.4.1-10.4.6). Kyoto, Japan.

Lateb, M., Masson, C., Stathopoulos, T. & Bédard, C. (2010). Numerical simulation of pollutant dispersion around a building complex. *Building and Environment, 45*(8), 1788-1798.

Letzel, O. L., Krane, M. & Raasch, S. (2008). High resolution urban large-eddy simulation studies from street canyon to neighborhoods scale. *Atmospheric Environment, 42*(38), 8770-8784.

Li, C., Li, X., Su, Y. & Zhu, Y. (2012). A new zero-equation turbulence model for microscale climate simulation. *Building and Environment, 47*, 243-255.

Lim, H. C., Thomas, T. G. & Casto, I. P. (2009). Flow around a cube in a turbulent boundary layer: LES and experiment. *Journal of Wind Engineering and Industrial Aerodynamics, 97*(2), 96-109.

Liu, C-H. , Cheng, W. C., Leung , T. C. Y. & Leung, D. Y.C. (2011). On the mechanism of air pollutant re-entrainment in two-dimensional idealized street canyons. *Atmospheric Environment, 45*(27), 4763–4769.

Liu, J., Srebric, J. & Yu, N. (2013). Numerical simulation of convective heat transfer coefficients at the external surfaces of building arrays immersed in a turbulent boundary layer. *International Journal of Heat and Mass Transfer, 61*, 209-225.

Ludwig, J. C. (Ed.). (2010). *PHOENICS-VR Reference Mannual*. London, UK: CHAM.

Maruyamaa, T., Taniguchib, T., Okazakic, M. & Taniikeb, Y. (2008). Field experiment measuring the approaching flows and pressures on a 2.4 m cube. Journal of Wind Engineering and Industrial Aerodynamics, 96(6-7), 1084-1091.

Mochida, A. & Lun, I. Y. F. (2008). Prediction of wind environment and thermal comfort at pedestrian level in urban area. *Journal of Wind Engineering and Industrial Aerodynamics, 96*(10-11), 1498-1527.

Montazeri, H. & Blocken, B. (2013). CFD simulation of wind-induced pressure coefficients on buildings with and without balconies: Validation and sensitivity analysis. *Building and Environment, 60*, 137-149.

Murakami, S. (1993). Comparison of various turbulence models applied to a bluff body. Journal of Wind *Engineering and Industrial Aerodynamics, 46*-47, 21-36.

Murakami, S. (1998). Overview of turbulence models applied in CWE-1997. *Journal of Wind Engineering and Industrial Aerodynamics, 74*(6), 1-24.

Nozawaa, K. & Tamurab, T. (2002). Large eddy simulation of the flow around a low-rise building immersed in a roughwall turbulent boundary layer. *Journal of Wind Engineering and Industrial Aerodynamics, 90*(10), 1151-1162.

Petchdee, P. & Chungloo, S. (2013). Improvement of Louvers and Openings of Factory Building to Remove Heat through Natural Wind. *Journal of Architectural/Planning Research and Studies, 10*(2), 31-44.

Qian, Y. (2004). *Development of an Algebraic Turbulence Model for Airflow and Contaminant Simulations around a Building. M.Sc. Thesis, Dept. of Architectural Engineering*. The Pennsylvania State University, Pennsylvania, USA.

Qian, Y. & Srebric, J. (2011). Development and Validation of an Algebraic Turbulence Model for Outdoor Airflow and Contaminant Simulations around a Building. *International Journal of Building, Urban, Interior and Landscape Technology, 1*(1), 43-51.

Ramponi, R. & Blocken, B. (2012a). CFD simulation of crossventilation for a generic isolated building: Impact of computational parameters. *Building and Environment, 53*, 34-48.

Ramponi, R. & Blocken, B. J. E. (2012b). CFD simulation of cross-ventilation flow for different isolated building configurations: validation with wind tunnel measurements and analysis of physical and numerical diffusion effects. *Journal of Wind Engineering and Industrial Aerodynamics, 104-106*, 408-418.

Remennikov, A. M. & Rose, T. A. (2005). Modelling blast loads on buildings in complex city geometries. *Computers and Structures, 83*(27), 2197-2205.

Roache, P. J. (1998). *Verification and validation in computational science and engineering*. New Mexico: Hermosa Publishers.

Roache, P. J. (1994). Perspective: A method for uniform reporting of grid refinement studies. *Journal of Fluids Engineering, 116*(3), 405-413.

Salim, S. M., Cheah, S. C. & Chan, A. (2011). Numerical simulation of dispersion in urban street canyons with avenue-like tree plantings: comparison between RANS and LES'. *Building and Environment, 46*(9), 1735-1746.

Santiago, J. L., Dejoan, A., Martilli, A., Martin, F. & Pinelli, A. (2010). Comparison between large-eddy simulation and Reynolds-averaged Navier–Stokes computations for the MUST field experiment. Part I: Study of the flow for an incident wind directed perpendicularly to the front array of containers. *Boundary-layer meteo rology, 135*(1). pp. 109-132.

Scaperdas, A. & Gilham, S. (2004). Thematic Area 4: Best practice advice for civil construction and HVAC. *The QNET-CFD Network Newsletter, 2*(4), 28-33.

Shi, R. F., Cuia, G. X., Wangb, Z. S., Xua, C. X. & Zhanga, Z. S. (2008). Large eddy simulation of wind field and plume dispersion in building array. Atmospheric *Environment, 42*(6), 1083-1097.

Stathopoulos, T. (1997). Computational wind engineering: Past achievements and future challenges. *Journal of Wind Engineering and Industrial Aerodynamics, 67-68*, 509-532.

Tantasavasdi, C., Sreshthaputra, A., Suwanchaiskul, A. & Pichaisak, M. (2009). Predicting Airflow in Naturally-ventilated Generic Houses. *Journal of Architectural/ Planning Research and Studies, 6*(1), 31-46.

Tominaga, Y., Mochida, A., Yoshie, R., Kataoka, H., Nozu, T. & Yoshikawa M, et al. (2008). AIJ guidelines for practical applications of CFD to pedestrian wind environment around buildings. *Journal of Wind Engineering and Industrial Aerodynamics, 96*(10-11), 1749–1761.

Tominaga, Y. & Stathopoulos, T. (2010). Numerical simulation of dispersion around an isolated cubic building: Model evaluation of RANS and LES. *Journal of Building and Environment, 45*(10), 2231-2239.

Tsuchiya, M., Murakami, S., Mochida, A., Kondo, K. & Ishida, Y. (1997). Development of a new kappa-epsilon model for flow and pressure fields around bluff body. *Journal of wind engineering and industrial aerodynamics, 67-68*, 169-182.

Xie, Z. & Castro, I. P. (2006). LES and RANS for turbulent flow over arrays of wall-mounted obstacles. *Flow, Turbulence and Combustion, 76*(3), 291-312.

Yakhot, A., Anor, T., Liu, H. P. & Nikitin, N. (2006). Direct numerical simulation of turbulent flow around a wallmounted cube: spatio-temporal evolution of largescale vortices. *Journal of Fluid Mechanics, 566*, 1-9.

Yoshihide, T., Akashi, M., Shuzo, M. & Satoshi, S. (2008). Comparison of various revised k-[epsilon] models and LES applied to flow around a high-rise building model with 1:1:2 shape placed within the surface boundary layer. *Journal of Wind Engineering and Industrial Aerodynamics, 96*(4), 389-411.

Zhang, Y. Q., Arya, S. P. & Snyder, W. H. (1996). A comparison of numerical and physical modeling of stable atmospheric flow and dispersion around a cubical building. *Atmospheric Environment, 30*(8), 1327-1345.